UCID- 20260

BEAM INJECTION IN THE TMX-U CENTRAL CELL

W. C. Turner

June 15, 1984

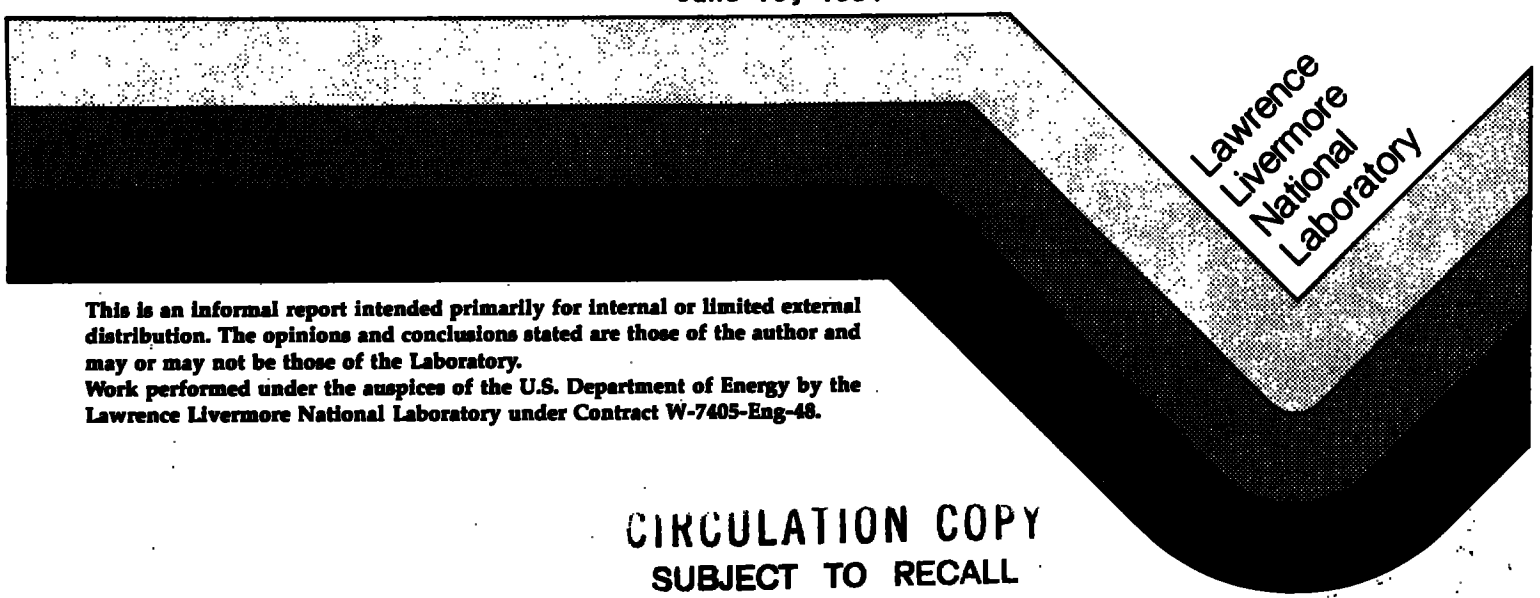

Work performed under the auspices of the U.S. Department of Energy by the Lawrence Livermore National Laboratory under Contract W-7405-Eng-48.

Printed in the United States of America
Available from
National Technical Information Service
U.S. Department of Commerce
5285 Port Royal Road
Springfield, VA 22161
Price: Printed Copy $; Microfiche $4.50

Page Range	Domestic Price	Page Range	Domestic Price
001-025	$ 7.00	326-350	$ 26.50
026-050	8.50	351-375	28.00
051-075	10.00	376-400	29.50
076-100	11.50	401-426	31.00
101-125	13.00	427-450	32.50
126-150	14.50	451-475	34.00
151-175	16.00	476-500	35.50
176-200	17.50	501-525	37.00
201-225	19.00	526-550	38.50
226-250	20.50	551-575	40.00
251-275	22.00	576-600	41.50
276-300	23.50	601-up[1]	
301-325	25.00		

[1]Add 1.50 for each additional 25 page increment, or portion thereof from 601 pages up.

BEAM INJECTION IN THE TMX-U CENTRAL CELL

W. C. Turner

ABSTRACT

Results pertaining to the recently modified beam-injection arrangement in the central cell of TMX-U are presented here. These modifications followed our observation that beam atoms injected perpendicular to the magnetic axis between the first two magnet-coil gaps give rise to trapped ions with midplane pitch angles lying in the intervals $68° < \theta < 78°$ and $59° < \theta < 65°$. These pitch-angle intervals are similar in value to the earlier arrangement of beams injected at the midplane at pitch angles of 58° and 70°. Normal injection at an off-midplane position has two advantages when compared with off-normal injection at the midplane. First, the unattenuated beam can be dumped in the first-injector region rather than in the plasma region. Second, the beams can be oriented with their long dimension horizontal rather than vertical. The first point allows a large improvement in central-cell vacuum conditions during beam injection, and the second provides improved beam-trapping efficiency in the core plasma. For the new beam-injection arrangement, we also displaced the beam-injection profiles vertically by one ion gyroradius to increase energy deposition at small radii. The advantages gained by the new beam orientation are considered in detail.

I. INTRODUCTION

This report considers the advantages of the new, off-midplane, perpendicular beam injection orientation in the central cell of TMX-U as opposed to the older arrangement with 70-deg beam injection at midplane. Our main findings are the following:

- During beam injection, the pressure in the plasma region is reduced by a predicted factor of 7.5 (from 1.5×10^{-5} to 2×10^{-6} Torr).

- The ratio of energetic beam atoms to cold gas atoms reaching the plasma region is increased from 0.71 to 5.1.
- The fraction of beam-injection energy trapped inside a core plasma radius r_c of 9 cm is increased by a factor of 2.9.
- The hot-ion density expected ispredicted as a function of warm-plasma density and electron temperature.

The predicted hot-ion parameters are given in Fig. 1 and in Table 1. Briefly, for a warm-plasma density n_w between 1 and 3 x 10^{12} cm^{-3}, the hot-ion density depends sensitively on n_w, and hot-ion losses are dominated by charge exchange. For a warm-plasma density greater than 3 x 10^{12} cm^{-3}, the hot-ion losses are dominated by scattering and drag. The hot-ion density is relatively insensitive to the magnitude of n_w. For conditions where 3 x 10^{12} < n_w < 1 x 10^{13} cm^{-3} and T_e = 500 eV, a hot-ion density $n_h \simeq$ 7 to 9 x 10^{12} cm^{-3} is predicted. If T_e = 125 eV, the predicted hot-ion density decreases to values between 3.5 and 5.5 x 10^{12} cm^{-3}.

Figure 2 indicates the key results that led to the new beam-injection arrangement. The midplane pitch angle is plotted in (a) and the corresponding magnetic-field strength is plotted in (b), both as a function of axial position of beam injection normal to the machine axis. Figure 1(a) shows that beam atoms injected between the first two magnet-coil gaps give rise to trapped ions with midplane pitch angles lying in the intervals 68° < θ < 78° and 59° < θ < 65°. The two beam-injection arrangements are shown in Fig. 3. The advantages gained by the new beam orientation are considered in the following sections.

II. VACUUM CONDITIONS WITH PREVIOUS 70-DEGREE BEAM INJECTION AT MIDPLANE

An analysis of the diffuse, streaming and beam-dump reflux of central-cell beams was done. The analysis, which is similar to our treatment of the end plugs,[1] also gives a value for the first wall-effective reflux coefficient. The main difference compared to the end plug analysis is that the central-cell plasma region was divided into three volumes (because of its relatively long length compared to the axial extent of beam gas input) whereas the plug plasma regions were treated as a single volume.

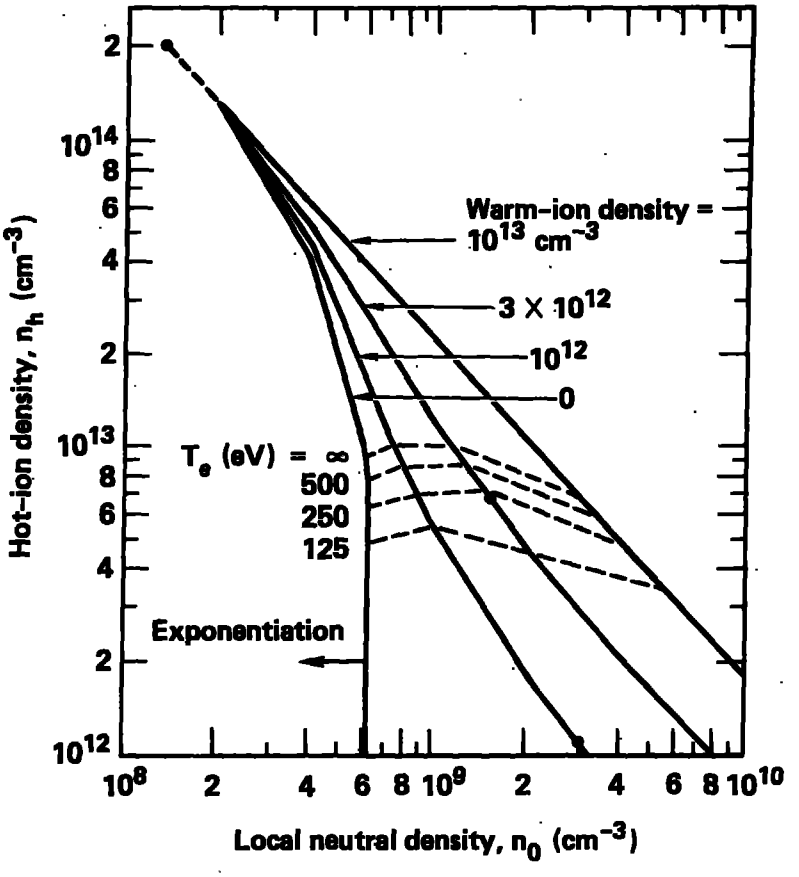

Fig. 1. Central-cell hot-ion density as a function of local neutral density.

Table 1.

Table 1. Summary of hot-ion plasma parameters.[a]

Case	n_w cm^{-3}	n_0 cm^{-3}	T_e eV	n_h cm^{-3}	E_h keV	β_h	P_{hw} (kW)	P_{he} (kW)	P_{cx}	τ_{cx}^{gas} ms	τ_{cx}^{beam} ms	τ_{ie} ms	τ_{ii} ms	τ_{ii}^{eff} ms
1.	1×10^{12}	3×10^{9}	∞	1.1×10^{12}	10	0.045	0.46	0	35.9	2.5	3.5	-	62.6	2×10^{8}
2.	3×10^{12}	1.5×10^{9}	∞	7×10^{12}	10	0.31	8.7	0	112	5.1	4.1	-	13.2	98
3.	1×10^{13}	1.3×10^{8}	∞	6.5×10^{12}	7.5	0.22	78.4	0	16.8	59	13.9	-	5.2	6.3
4.	1×10^{12}	3×10^{9}	500	1.1×10^{12}	10	0.045	0.46	0.40	35.9	2.5	3.5	224	62.6	2×10^{8}
5.	3×10^{12}	1.5×10^{9}	500	7×10^{12}	10	0.31	8.7	12.2	112	5.1	4.1	47	13.2	98
6	1×10^{13}	1.3×10^{8}	500	5.8×10^{12}	6.8	0.17	73.4	26.9	13.6	59	13.8	29.7	4.6	5.5
7.	1×10^{12}	3×10^{9}	250	1.1×10^{12}	10	0.045	0.46	1.14	35.9	2.5	3.5	79	62.6	2×10^{8}
8.	3×10^{12}	1.5×10^{9}	250	7×10^{12}	10	0.31	8.7	34.4	112	5.1	4.1	16.6	13.2	98
9.	1×10^{13}	1.3×10^{8}	250	4.7×10^{12}	5.9	0.12	63.9	49.8	9.6	59	13.7	11.3	4.0	4.7
10.	1×10^{12}	3×10^{9}	125	1.1×10^{12}	10	0.045	0.46	3.2	35.9	2.5	3.5	28	62.6	2×10^{8}
11.	3×10^{12}	1.5×10^{9}	125	4.4×10^{12}	5.2	0.11	19.1	58.5	91.2	5.1	10.1	7.0	6.7	9.4
12.	1×10^{13}	1.3×10^{8}	125	3.4×10^{12}	4.6	0.07	52.4	72.4	5.4	59	13.5	4.4	3.1	3.4

[a]Definitions of symbols used are given in Appendix.

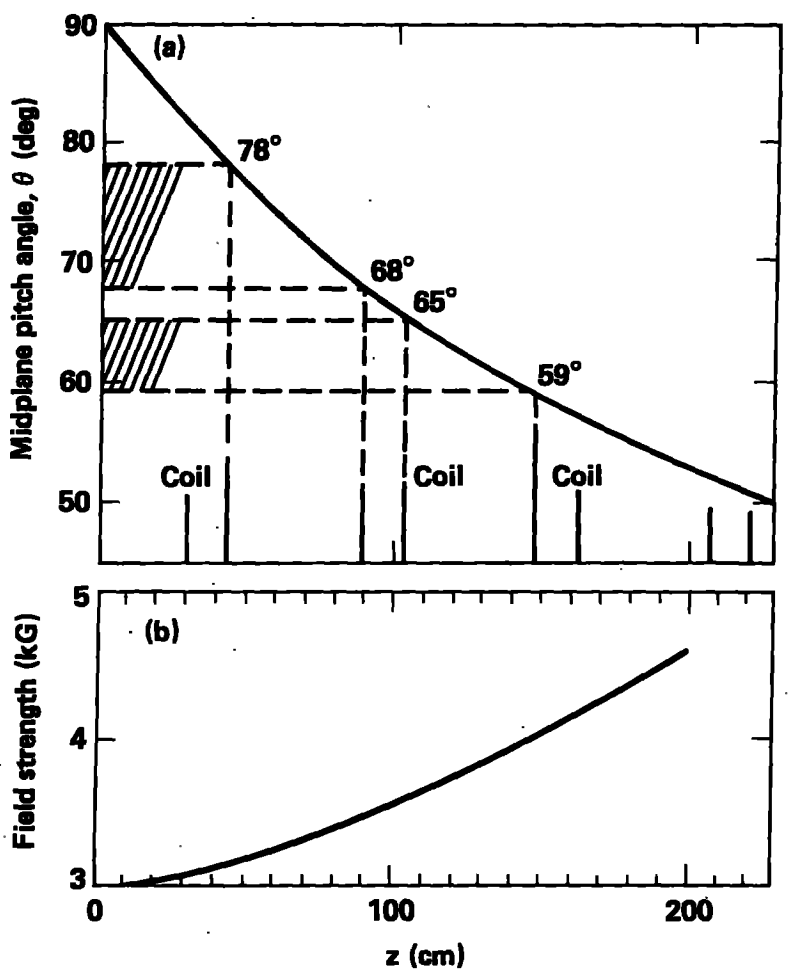

Fig. 2. Midplane pitch angle (a) and field strength (b) as a function of the 90-deg axial injection position.

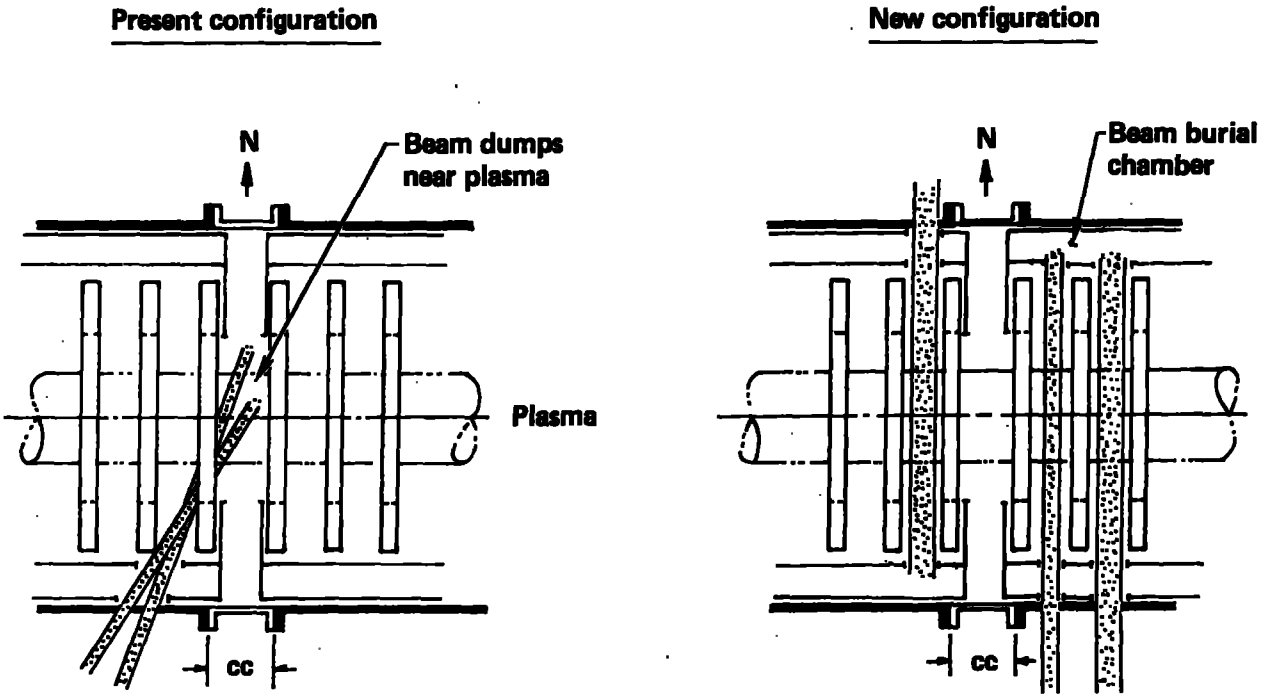

Fig. 3. Old configuration (a) and the new recently modified (b) beam-injection arrangement in the TMX-U central cell. The new configuration provides vacuum improvements, as beams will dump into separate baffled chamber.

The three-volume model of the central-cell plasma region is shown in Fig. 4. The equations for the model are

$$V_1 \frac{dP_1}{dt} = Q_1 - S_1 P_1 - 2\, C_{12}(P_1 - P_2) \quad , \tag{1}$$

$$V_2 \frac{dP_2}{dt} = Q_2 - S_2 P_2 + C_{12}\,(P_1 - P_2) \quad . \tag{2}$$

Here, as in our earlier analysis,[1] gas flow from the second injector region into the plasma region is included in the Q values, gas flow from the plasma region into the second injector region is included in the calculated S values. Calculation of Q_1 from the measured fast-ionization gauge (FIG) pressure in the central-cell disc region will give the beam gas inputs as well as wall reflux in this region. Because the beam dumps in the disc region, and the warm-wall entrance apertures are adjacent to the disc region, all of the direct beam gas input is assumed to be in the disc region, and none in the two outer regions. In the two outer regions, Q_2 includes gas fueling from the central-cell gas box and transition gas feeds as well as wall reflux in these regions. Since we only have measurements of P_1 and not P_2, Eq. (2) is used to eliminate P_2, arriving at

$$Q_1 = V_1 \frac{dP_1}{dt} + (S_1 + 2C_{12})\, P_1 - 2C_{12}\, e^{-t/\tau_2} \int_0^t e^{t'/\tau_2} \left(\frac{Q_2}{V_2} + \frac{C_{12} P_1}{V_2} \right) dt' \quad , \tag{3}$$

where

$$\tau_2 = \frac{V_2}{S_2 + C_{12}} \quad .$$

In general, Q_1 is given by

$$Q_1 = Q_S + Q_D + Q_B + Q_w$$

where Q_S is streaming-beam gas input, Q_D is diffuse-beam gas input from second injector region, Q_B is beam-dump reflux, and Q_w is wall reflux. The streaming-gas input Q_S is calculated from the known inputs to the beam arc chambers and from geometry. The beam diffuse gas Q_D is measured with an arc only shot, beam-dump reflux Q_B is measured with arc plus extracted beam, and wall reflux is measured with a plasma shot.

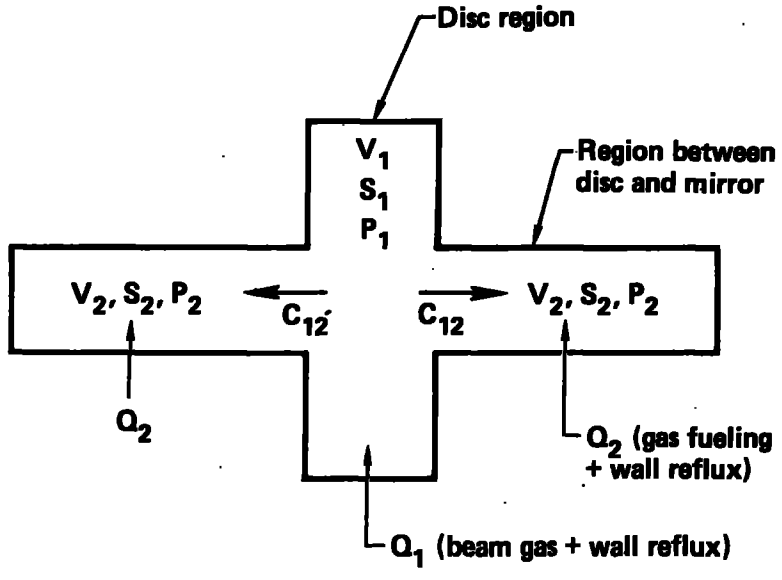

$V_1 = 5.9 \times 10^3$ litre

$V_2 = 3.4 \times 10^3$ litre

$C_{12} = 3.5 \times 10^5$ litre/s

	No plasma	With plasma
S_1	2.0×10^5 litre/s	3.8×10^5 litre/s
S_2	2.3×10^5 litre/s	6.0×10^5 litre/s

Fig. 4. Three-volume model of central-cell plasma region.

In Fig. 5, we give FIG data for four shots on 12/14/83, namely S-13 [arcs + accel (extracted beam)], S-14 (arcs only), S-15 (plasma shot with central-cell beams), and S-18 (plasma shot without central-cell beams). The four central-cell 70° beams were used for all of these shots except S-18; the 58° beam-attenuation detector (BAD) beam was not used. Note in Fig. 4 that on the shot without central-cell beams (S-18), the increase in the FIG pressure in the disc region, $\Delta P = 2 \times 10^{-7}$ Torr, is much less than for the other three shots. Therefore, as far as the central cell disc region is concerned, gas fueling inputs are negligible compared to the beams. For this reason, when using Eq. (3) to analyze the first three shots, we set $Q_2 = 0$. Wall reflux in Region 2 is treated by inclusion in the effective pumping speed. That is

$$S_2 = S_w + (1 - f)\, S_p$$

where S_w and S_p are the wall and plasma pumping speeds in Region 2, and $f = 0.75$ is the wall reflux parameter set equal to the value measured in the plugs.[2] Second, the pressure data can be fit with linear or exponential functions,

$$\begin{aligned} P_1 &= \alpha t \\ \alpha &= 4.13 \times 10^{-4} \text{ Torr/s} \quad \text{(Shot S-13)} \\ \alpha &= 7.95 \times 10^{-5} \text{ Torr/s} \quad \text{(Shot S-14)} \end{aligned} \tag{4}$$

$$\begin{aligned} P_1 &= \beta\,[1 - e^{-\gamma t}] \\ \beta &= 3.9 \times 10^{-5} \text{ Torr} \quad \text{(Shot S-17)} \\ \gamma &= 10.6 \text{ s}^{-1} \end{aligned} \tag{5}$$

Inserting these two functional forms in Eq. (3) then gives

$$Q_1 = \alpha V_1 + (S_1 + 2C_{12})\,\alpha t - 2C_{12}\alpha\tau_2 \frac{C_{12}\tau_2}{V_2}\left[\left(\frac{t}{\tau_2} - 1\right) + e^{-t/\tau_2}\right] \tag{6}$$

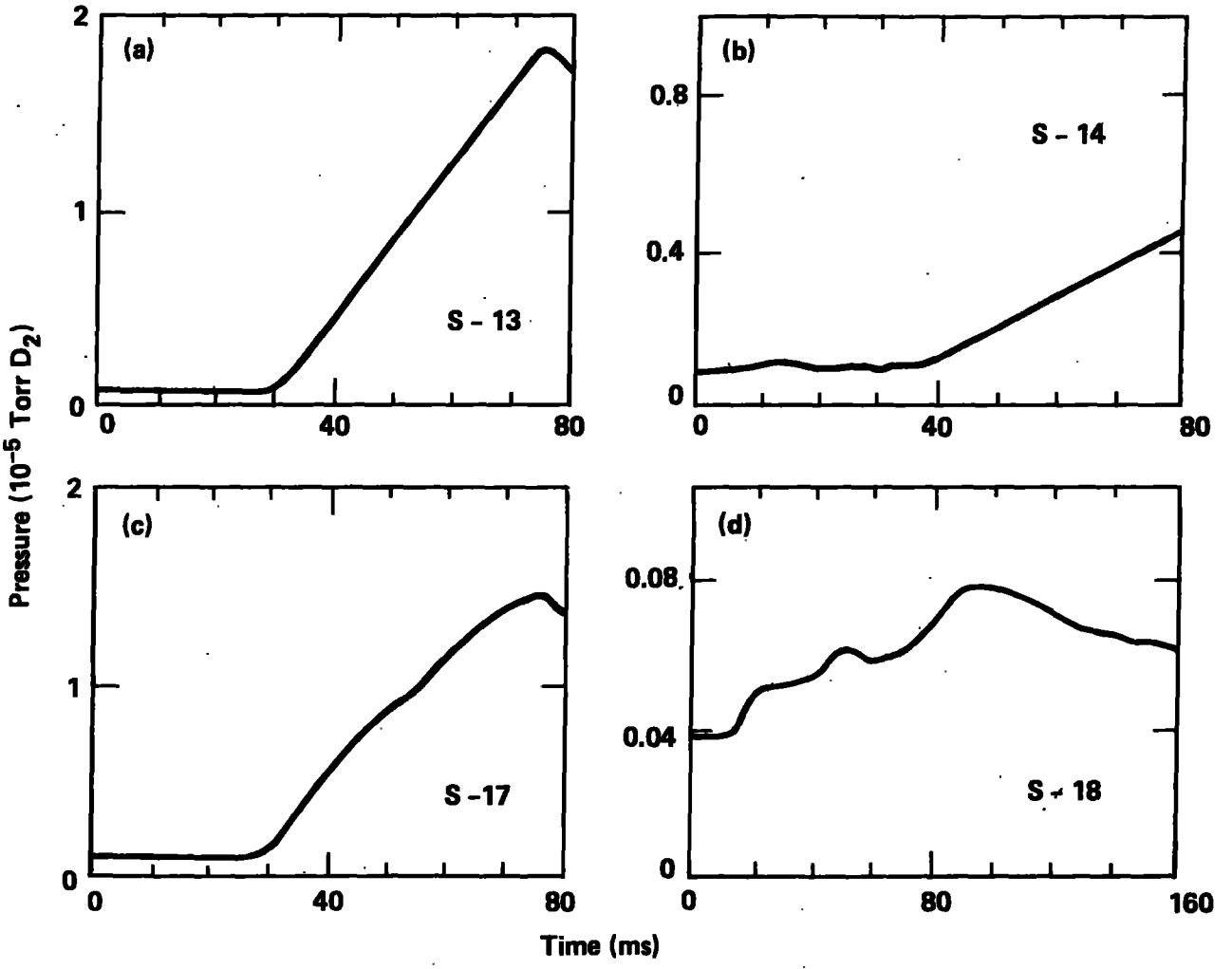

Fig. 5. Central-cell fast-ionization gauge (FIG) data for shots of 12-14-83 and four 70-deg beams. (a) Shot 13, arcs + accel (extracted beam). (b) Shot 14, arcs only. (c) Shot 17, plasma shot with central-cell beams. (d) Shot 18, plasma shot without beams. East and west transition gas injection was 20 Torr•litre/s for 5 to 25 ms; central-cell gas box injection was 28 Torr•litre/s for 25 to 65 ms).

$$Q_1 = V_1\beta\gamma\, e^{-\gamma t} + (S_1 + 2C_{12})\,\beta\,(1 - e^{-\gamma t})$$

$$- 2C_{12}\beta\,\frac{C_{12}\tau_2}{V_2}\left[(1 - e^{-t/\tau_2}) - \frac{e^{-\gamma t} - e^{-t/\tau_2}}{1 - \gamma\tau_2}\right] \qquad (7)$$

for the linear and exponential functions respectively.

Inserting the appropriate numerical values in Eqs. (6) and (7) for shots S-13, -14 and -17 gives the individual gas inputs shown in Fig. 6. The streaming-gas input is calculated to be 0.69 Torr•litre/s, and must be subtracted from the data to isolate the diffuse gas contribution. Figure 6 shows that the beam-dump reflux is the largest contributor to pressure rise in the central cell, reaching 9.5 Torr•litre/s late in the shot.

The beam gas inputs at 70 ms are summarized in Table 2. The table shows that, late in time, the ratio of energetic beam atoms to cold gas atoms reaching the plasma is only 0.8, compared to 10.9 that was achieved for the end-plug sloshing beams.[2] Also, late in time, the ratio of gas atoms released from the wall to beam atoms striking the wall is about 1.0.

Finally, a plot of wall reflux Q_w versus pressure (see Fig. 7) shows that Q_w is linearly dependent on pressure as observed in the end plugs.[2] If Q_w is parameterized[2] as

$$Q_w = Q_1 + f\,S_p P$$

$$f = 2(1 - p_{ion})\gamma_w$$

then for 10 eV < T_e < 20 eV, f = 0.46 and γ_w = 0.4 to 0.65 .

III. IMPROVEMENT IN VACUUM CONDITIONS PREDICTED WITH NEW OFF-MIDPLANE PERPENDICULAR-BEAM INJECTION

In this section we estimate the steady-state central-cell gas inputs and pressure obtained with the new off-midplane perpendicular injection. As in our previous analysis of FIG data obtained with the old 70° injection, we

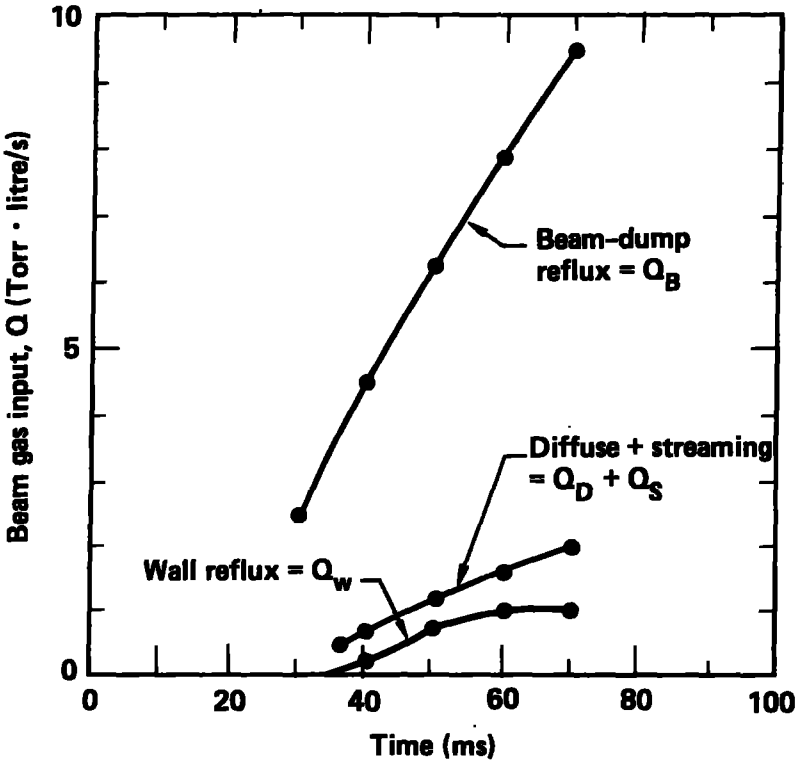

Fig. 6. Central-cell beam gas-input data of 12-14-83 for TMX-U Shots 13, 14, and 17.

Table 2. Central-cell beam gas inputs for each of four, central-cell, 70-deg beams at t = 70 ms.

Beam parameter	Value
Gas input (Torr•litre/s):	
Diffuse	1.97 - 0.69 = 1.28
Streaming	0.69
Dump reflux	9.49
Total	11.46
I_{beam} (A)	103
I_{beam}/I_{gas}	0.8
$\Upsilon_{dump\ reflux}$	$\frac{9.49 \times 11.3}{103} = 1.04$

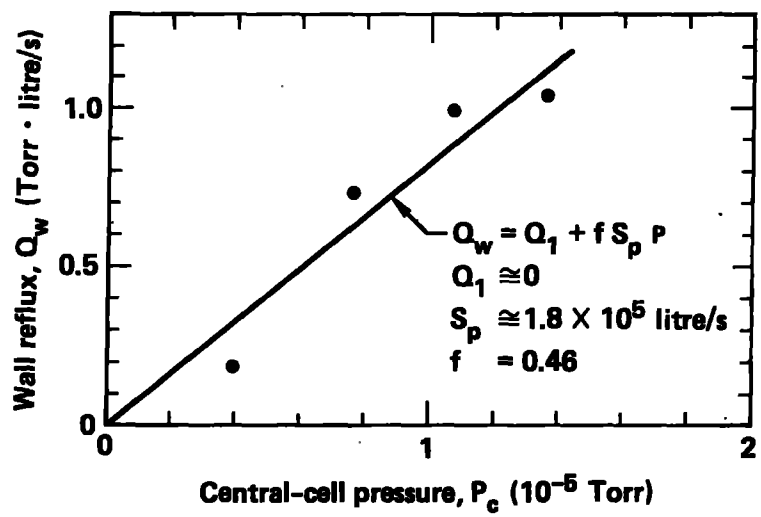

Fig. 7. Wall reflux Q_w as a function of central-cell pressure.

treat the plasma region as three distinct volumes. However, since we now wish to calculate gas flows into the plasma region, rather than deduce them from FIG measurements, we must include additional volumes to represent the first and second injector regions. This leads to the seven-volume model of Fig. 8, where symmetry was invoked to reduce the number of different volumes to four. In cases where asymmetry exists in the actual experiment--such as the seventh or BAD beam east of the midplane or where baffling was added to the east beams to avoid scrape-off on the slot ICRH antenna--average values are assigned to the symmetrized model. The steady-state pumping equations are the following:

$$Q_1 = S_1P_1 + C_{12}(P_1 - P_2) \quad ,$$

$$Q_2 = S_2P_2 + C_{12}(P_2 - P_1) + C_{23}(P_2 - P_3) \quad ,$$

$$Q_3 = S_3P_3 + C_{23}(P_3 - P_2) + C_{23}P_3 - C_{43}P_4 \quad ,$$

$$Q_4 = S_4P_4 + C_{43}P_4 - C_{34}P_3 \quad , \tag{8}$$

where

Q_1 = wall reflux gas,

Q_2 = wall reflux + beam streaming gas,

Q_3 = beam and streaming scrape-off gas,

Q_4 = gas input to arc chambers + beam dump reflux.

In the above equations, by definition $P_j = n_jkT$ with T = 300 K, whereas the different molecular speeds due to surfaces at liquid-nitrogen-temperature are taken into account in calculating the C_{ij} values. Numerical values for S_j, C_{ij} and Q_j in Eq. (8) are given in Table 3. Values given correspond to the three types of experimental data shots--plasma, arcs only, arcs + accel--so that comparisons can be made with data in the previous section and with data from the next run. For the arcs only and arcs + accel shots in Table 3, only

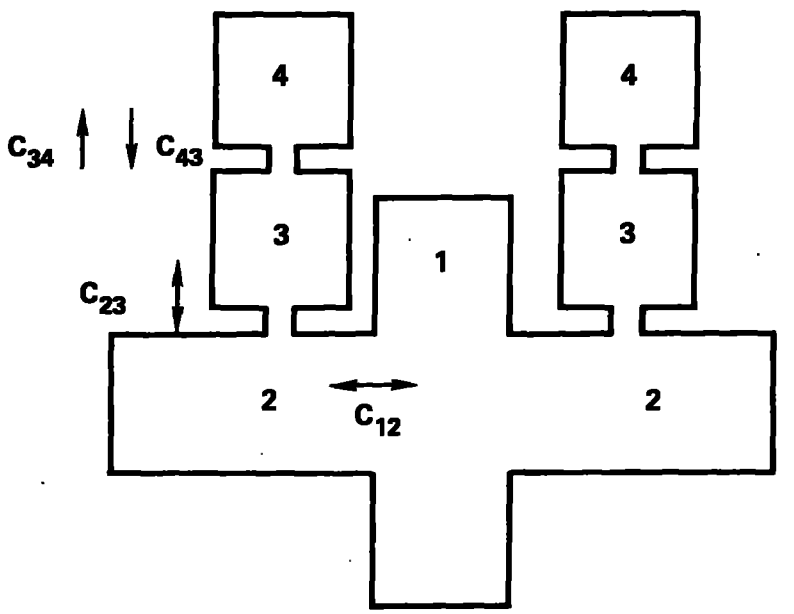

Fig. 8. Symmetric model for estimating central-cell vacuum conditions.

Table 3. Pumping speeds, conductances, and gas inputs for central-cell vacuum calculations.

Quantity	Plasma shot	Arcs only	Arcs + accel
Pumping speed (litre/s):			
S_1	3.8×10^5	2.01×10^5	2.01×10^5
S_2	1.61×10^6	1.28×10^5	1.28×10^5
S_3	1.2×10^6		
S_4	1.2×10^6		
Conductance (litre/s):			
C_{12}	3.5×10^5		
C_{23}	1.04×10^5		
C_{34}	1.35×10^5		
C_{43}	6.8×10^4		
Gas inputs (Torr·litre/s):			
Q_1	1.80×10^5 fP_1	0.0	0.0
Q_2	1.45×10^6 fP_2 + 1.10	0.0	0.20
Q_3	5.53	1.52	5.53
Q_4	81.1	86.0	81.8

those quantities that differ from those of the plasma shot are listed; otherwise the values are the same as for the plasma shot.

In Eq. (8), the gas input to the arc chambers and the beam-dump reflux are treated as if they originate in the same volume (4) and flow from the first to second injector regions through the same conductance ($=C_{43}$), even though physically they are on opposite sides of the machine. This is justified because the mean distance a gas molecule travels in the direction parallel to the liquid-nitrogen-temperature pumping surfaces before sticking (=140 cm) is comparable to half the mean circumference of the liquid-nitrogen-filled liners (=220 cm). This model gives a somewhat more conservative estimate of diffuse gas flow into the plasma region than if the beam source and dump sides were treated separately. As discussed later, the pressure in the plasma region is dominated by wall reflux and streaming gas, so our final result only weakly depends on the assumption that the arc-chamber gas and dump reflux originate in the same volume.

In Table 3, the pumping speeds S_1 and S_2 and the conductance C_{12} are taken from Fig. 4. The pumping speeds S_3 and S_4 of the first and second injector regions are calculated from liquid-nitrogen liner data in Table 4 in Ref. 1. A sticking coefficient of 0.2 is assumed on titanium-gettered liquid-nitrogen-cooled surfaces. Only the axial extent of Liners 5 and 6 or 9 and 10 in the referenced Table 4 are included to calculate S_3, and pumping by gettered warm surfaces is neglected. Because of all the magnet and warm-wall structure in Region 3, a molecular velocity v of 1.25×10^5 cm/s (300 K) is used to calculate S_3. Region 4 is bounded by liquid-nitrogen-cooled liners on the inside and outside, so a velocity of 0.625×10^5 cm/s (80 K) is used to calculate S_4. The factor of 2 difference in velocity between Regions 3 and 4 is compensated by a factor of 2 difference in gettered liquid-nitrogen-cooled area, so $S_1 = S_2$.

The conductances C_{23}, C_{34}, and C_{43} are calculated from measured sizes of aperture holes and ducts and averaged over the east and west halves of the central-cell. The differences between east and west values is $\leq$25%.

No direct gas inputs are present in disc liner Region 1 in Fig. 8, so the only contribution to Q_1 is wall reflux. In our earlier notation[2] describing the end plugs,

Table. 4. Steady-state pressure P for the different shot types.

Shot type / Pressure	Plasma (f = 0.75) (Torr)	Arc only (Torr)	Arc + accel (Torr)
P_1	1.4×10^{-6}	0.8×10^{-6}	1.7×10^{-6}
P_2	2.4×10^{-6}	1.3×10^{-6}	2.6×10^{-6}
P_3	7.0×10^{-6}	4.4×10^{-6}	7.1×10^{-6}
P_4	6.5×10^{-5}	6.8×10^{-5}	6.5×10^{-5}

$$Q_1 = f\, S_{p_1} P_1$$

where

$$f = 2\,(1 - p_{ion})\,\gamma_w \quad .$$

The parameter p_{ion} is the probability that an atom incident as a molecule on the plasma surface is ionized, γ_w is the number of D_2 molecules released from the wall per incident atomic D^0, and S_p is the black-surface pumping speed of the plasma. The parameter f is included as a parameter in Table 3. Experimentally, our best documented value is f = 0.75.[2] With no plasma present, recycling is absent and $Q_1 = 0$, as in the last two columns of Table 3.

On a plasma shot, Q_2 consists of a wall-reflux term proportional to P_2, similar to Q_1, plus an additional constant 1.1 Torr•litre/s. The constant term is the sum of arc-chamber streaming gas (0.61 Torr•litre/s), beam-dump streaming gas (0.22 Torr•litre/s), and wall reflux of charge-exchange atoms (0.25 Torr•litre/s). With arcs only, Q_2 = 0.20 Torr•litre/s because of scrape-off of streaming gas from the beam dump as it passes back through the plasma region.

On plasma shots and arcs + accel shots, the gas input Q_3 to the second injector region consists of beam scrape-off (1.49 Torr•litre/s), scrape-off of streaming gas from the arc chambers (1.52 Torr•litre/s), and scrape-off of streaming gas from the beam dumps (2.52 Torr•litre/s). With arcs only, the beam terms are absent.

The gas input Q_4 to the first injector region consists mainly of the gas that is fed into the arc chambers. We assume 25 Torr•litre/s for each beam, and small corrections are made for streaming into other regions. Where the beams dump in the first injector region, we assume in all of these calculations that the beam recycles with a unity reflux coefficient.

Using the values in Table 3, we solve Eq. (8) for the pressure in each of the regions. The results are tabulated in Table 4, where we have assumed the best experimental value, f = 0.75, for wall reflux on the plasma shot. We can compare the plasma-shot calculated pressures of 1.4×10^{-6} and 2.4×10^{-6} Torr for P_1 and P_2, respectively, with the experimental results for the old central-cell beam orientation, where P_1 equals 1.5×10^{-5} Torr (Fig. 5). We

see that a large improvement in central-cell pressure is predicted in the region where central-cell beams are trapped. Specifically, the bounce-averaged pressure between the initial turning points of the central-cell beam-injected ions has been reduced by a factor of

$$\frac{1.5 \times 10^{-5}}{1/3\ (1.4 \times 10^{-6}) + 2/3\ (2.4 \times 10^{-6})} = 7.3 \quad ,$$

because the ions spend roughly twice as much time in Region 2 as in Region 1.

From the arcs only shot in Table 4, we calculate the diffuse gas input from the arc chambers;

$$2C_{32}P_3 = 0.90 \text{ Torr} \cdot \text{litre/s} \quad \text{(diffuse gas)} \quad ,$$

where the factor of 2 includes both plasma regions that are labeled 2 in Fig. 8. Similarly, from the arcs + accel shot and after subtracting diffuse flow from the arc chamber, we find the gas flux that is due to diffuse flow from the beam dumps to be

$$2C_{32}P_3 - 0.90 = 1.48 - 0.90$$

$$= 0.58 \text{ Torr} \cdot \text{litre/s} \quad \text{(dump reflux)} \quad .$$

For the plasma shot in Table 4, it is interesting that if we calculate the total diffuse-gas input to the plasma region, we obtain

$$2C_{32}P_3 = 1.46 \text{ Torr} \cdot \text{litre/s}$$

which is very close to the value obtained for the arc + accel shot. This justifies our experimental procedure of deducing beam diffuse gas from background shots (arcs only, arcs + accel) and then subtracting from a plasma shot to isolate wall reflux.

This procedure works because pressure in the outer injector regions is relatively insensitive to pressure variations in the plasma region. This is not too apparent from the plasma and arc + accel shots in Table 4, because the plasma-region pressure only changes by 20%. However, it becomes more apparent when the wall-reflux coefficient is varied (see Fig. 9), which causes pressure in the plasma regions to change by a factor of approximately 5, while on the

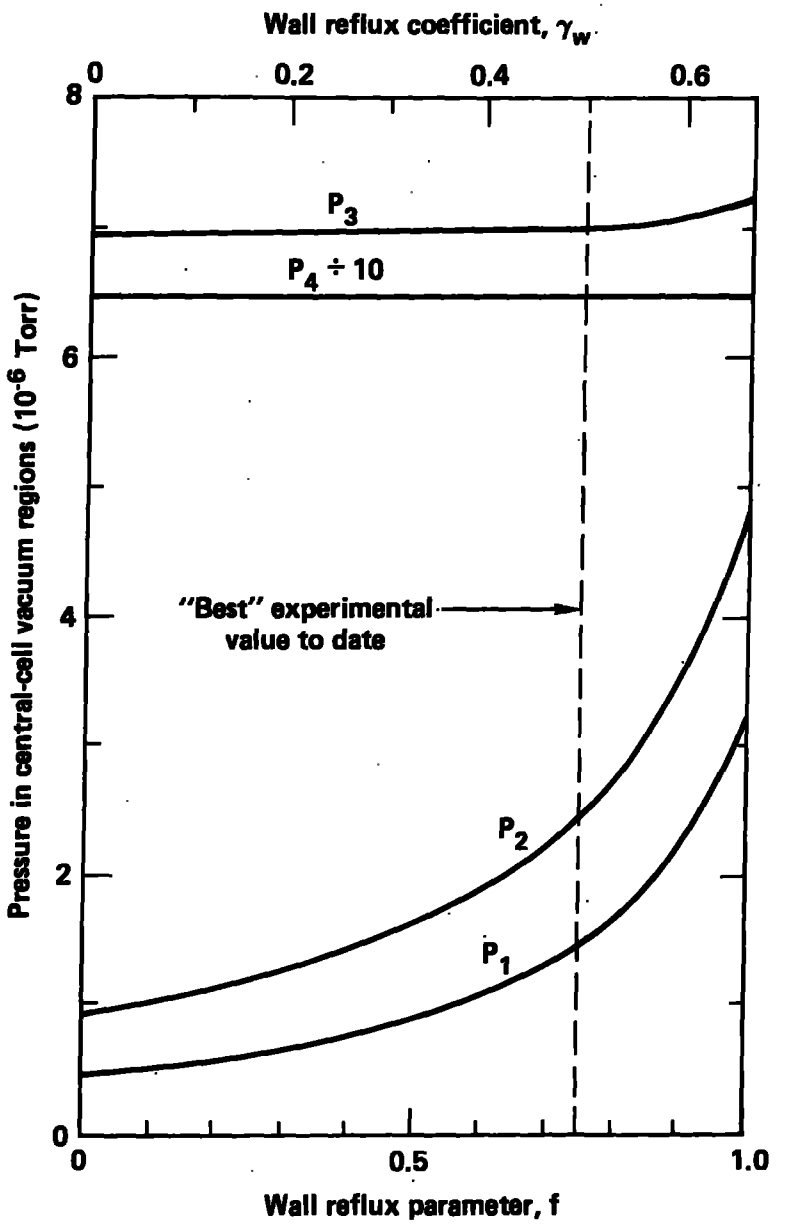

Fig. 9. Pressure in the vacuum regions of the central cell as a function of the wall reflux parameter f.

other hand the pressure P_3 in the second injector region changes by only 4%, and the pressure P_4 in the first injector region not at all.

Returning to Table 4, we calculate the wall reflux for the plasma shot,

$$2\ f\ S_p P_2 + f\ S_p P_1 = 6.05\ \text{Torr}\cdot\text{litre/s} \quad .$$

These results are summarized in Table 5 together with corresponding results from the previous beam-injection arrangement. For the old 70° injection at the midplane, the experimental results of Table 2 for a total of four beams were scaled up to seven beams so a direct comparison could be made with the new data. We see that the total gas input per beam to the plasma region is predicted to be improved by a factor 7.3 (20.06/2.76). The ratio of energetic-beam atoms to cold-gas atoms reaching the plasma is increased by the same factor.

Finally, because wall reflux is predicted to be the dominant gas load in the plasma region, we calculate the solution for Eq. (8) as the reflux parameter f varied from zero to 1.0. In Fig. 9, the pressure in each region is plotted as a function of f. The wall reflux coefficient γ_w (shown on top horizontal scale of the figure) is for an edge plasma T_e of 10 eV. The pressures in the plasma region P_1 and P_2 increase rapidly as f exceeds the "best" experimental value 0.75, and no steady-state solution exists for f greater than 1.0. The best we could hope for by reducing f below its present best value of 0.75 would give a factor-of-2 reduction in pressure. As stated earlier, the pressures in the first and second injector regions are relatively insensitive to the variations of P_1 and P_2, thus providing justification for our experimental subtraction method of deducing beam gas and wall reflux from FIG measurements with plasma and background shots.

IV. IMPROVEMENT IN BEAM-TRAPPING EFFICIENCY

In this section we estimate the fraction of beam-injected atoms that are trapped with their guiding centers lying inside a radius r. The calculation is done for the two beam orientations shown in Fig. 10. The old orientation, with the long dimension (b = 40 cm) of the beam footprint vertical and centered on the machine axis, is shown in Fig. 10(a). Figure 10(b) shows the new

Table 5. Gas inputs to central-cell to compare old and new beam orientations.

Source	70-deg injection at midplane (old, experimental)[a]	90-deg injection off midplane (new, calculated)
Beam Gas (Torr•litre/s):		
Diffuse	2.24	0.90
Streaming	1.21	1.28
Dump Reflux	16.61	0.58
Total	20.06	2.76
$I_{beam(A)}$	160	160
I_{beam}/I_{gas}	0.71	5.1
Wall reflux (Torr•litre/s)	--	6.05

[a]Scaled from 4 to 7 beams to compare with new arrangement.

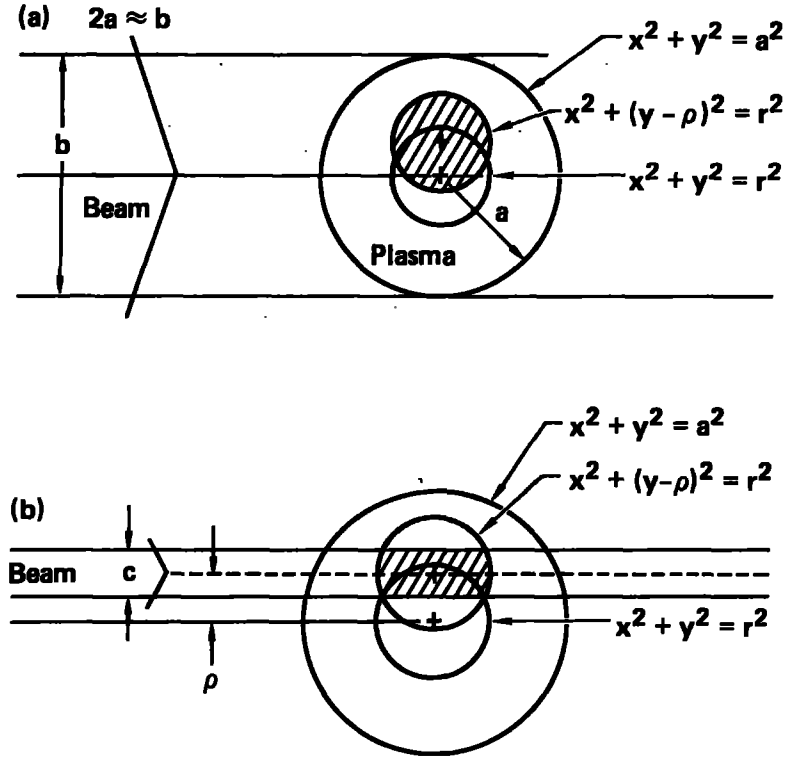

Fig. 10. The two beam orientations used for calculating trapping of beam-injected atoms. (a) Vertical orientation (old). (b) Horizontal orientation (new).

orientation with the short dimension (c = 6 cm) of the beam footprint is vertical and centered one gyroradius off the machine axis to enhance the energy deposited at small radii. In the thin plasma limit, $4/3\ a\ n_0\ \sigma \ll 1$, or $n_0 \ll 2.5 \times 10^{13}\ cm^{-3}$ for a = 20 cm and $\sigma = 1.5 \times 10^{-15}\ cm^{-2}$, the fraction of beam-injected atoms that are trapped with their guiding centers lying inside a radius r is given by

$$f(r) = \frac{2\sigma \int_{y=\rho-r}^{\rho+r} dy \frac{dI}{dy} \int_{x=0}^{[r^2-(y-p)^2]^{1/2}} n(x,y)\, dx}{\int_{-\infty}^{+\infty} dy \frac{dI}{dy}} \qquad (9)$$

In Eq. (9) integration extends over a circle of radius r that is displaced upward by a gyroradius ρ. To make the calculation analytically tractable, we consider a parabolic density profile

$$n(x,y) = \hat{n}\left(1 - \frac{x^2}{a^2} - \frac{y^2}{a^2}\right) \quad , \quad x^2 + y^2 < a^2$$

$$= 0 \quad , \qquad x^2 + y^2 > a^2 \qquad (10)$$

and rectangular beam profiles

$$\frac{dI}{dy} = \frac{I}{b} \quad , \quad -\frac{b}{2} < y < +\frac{b}{2} \ ;$$

$$= 0 \quad , \quad y < -\frac{b}{2} \quad , \quad y > \frac{b}{2} \ ;$$

$$\frac{dI}{dy} = \frac{I}{c} \quad , \quad \rho - \frac{c}{2} < y < \rho + \frac{c}{2} \ ;$$

$$= 0 \quad , \quad y < \rho - \frac{c}{2} \quad , \quad y > \rho + \frac{c}{2} \ . \qquad (11)$$

If we take into account the integration boundaries imposed by these profiles, the expressions for f(r) are given in the following equations.

Vertical Orientation:

$0 < r < a - \rho$

$$f_V(r) = \frac{2\hat{n}\sigma}{b} \int_{y=\rho-r}^{\rho+r} dy \int_{x=0}^{[r^2-(y-\rho)^2]^{1/2}} \left(1 - \frac{x^2}{a^2} - \frac{y^2}{a^2}\right)$$

$$= \frac{2\hat{n}\sigma}{b} \pi r^2 \left(1 - \frac{\rho^2}{a^2} - \frac{1}{2}\frac{r^2}{a^2}\right) . \qquad (12)$$

$a - \rho < r < a + \rho$

$$f_V(r) = \frac{2\hat{n}\sigma}{b} \int_{y=\rho-r}^{a^2+\rho^2-r^2/2\rho} dy \int_{x=0}^{[r^2-(y-\rho)^2]^{1/2}} dx \left(1 - \frac{x^2}{a^2} - \frac{y^2}{a^2}\right) . \qquad (13)$$

Horizontal Orientation:

$0 < r < \frac{c}{2}$

$$f_H(r) = \frac{2\hat{n}\sigma}{c} \int_{y=\rho-r}^{\rho+r} dy \int_{x=0}^{[r^2-(y-\rho)^2]^{1/2}} dx \left(1 - \frac{x^2}{a^2} - \frac{y^2}{z^2}\right) ,$$

$$= \frac{2\hat{n}\sigma}{c} \pi r^2 \left(1 - \frac{\rho^2}{a^2} - \frac{1}{2}\frac{r^2}{a^2}\right) . \qquad (14)$$

$\frac{c}{2} < r < (a^2 - \rho^2 - \rho c)^{1/2}$

$$f_H(r) = \frac{2\hat{n}\sigma}{c} \int_{y=\rho-c/2}^{\rho+c/2} dy \int_{x=0}^{[r^2-(y-\rho)^2]^{1/2}} dx \left(1 - \frac{x^2}{a^2} - \frac{y^2}{a^2}\right)$$

$$= \frac{2\hat{n}\sigma}{c} \left(1 - \frac{\rho^2}{a^2} - \frac{1}{2}\frac{r^2}{a^2}\right) \left[c\left(r^2 - \frac{c^2}{4}\right]^{1/2} + 2r^2 \sin^{-1}\left(\frac{c}{2r}\right)\right]$$

$$+ \frac{1}{3}\frac{\hat{n}}{a^2}\left(r^2 - \frac{c^2}{4}\right)^{3/2} . \qquad (15)$$

$$(a^2 - \rho^2 - \rho c)^{1/2} < r < (a^2 - \rho^2 + \rho c)^{1/2}$$

$$f_H(r) = \frac{2\hat{n}\sigma}{c} \int_{y=\rho-c/2}^{\rho+c/2} dy \int_{x=0}^{[r^2-(y-\rho)^2]^{1/2}} dx \left(1 - \frac{x^2}{a^2} - \frac{y^2}{a^2}\right)$$

$$+ \frac{2\hat{n}\sigma}{c} \int_{y=a^2+\rho^2-r^2/2\rho}^{\rho+c/2} dy \int_{x=0}^{(a^2-y^2)^{1/2}} dx \left(1 - \frac{x^2}{a^2} - \frac{y^2}{a^2}\right) \quad . \qquad (16)$$

Some of the above formulas have been left in integral form, because the integrated expressions, which have been worked out in detail, are rather cumbersome.

In Fig. 11(a) for a = 20 cm, b = 40 cm, c = 6 cm, and ρ = 6 cm, we plot $f_H(r)$ and $f_V(r)$, normalized to $\sigma n_0 a^2$, as a function of normalized radius r/a. The ratio f_H/f_V describes the relative improvement in beam trapping for the horizontal over the vertical orientation [see Fig. 11(b)]. For small radii, r < c/2 = 3 cm, f_H/f_V = b/c = 6.7. At larger radii, f_H/f_V decreases, because the beam height is less than the diameter of the trapping region for horizontal aiming. However, the gain is still sizable;

f_H/f_V = 4.2 at r = ρ = 6 cm,

= 2.65 at r = a/2 = 10 cm,

= 1.5 at r = a = 20 cm.

V. PREDICTION OF HOT-ION DENSITY

In this last section, we calculate the hot-ion density obtained by neutral-beam injection into the central cell. A warm-plasma background density described by

$$n_w = \hat{n}_w \left(1 - \frac{r^2}{a^2}\right) \quad ,$$

with a = 20 cm, is assumed to be present for trapping beam-injected ions. The hot-ion density is calculated inside a core radius defined by r = ρ + c/2 = 9 cm,

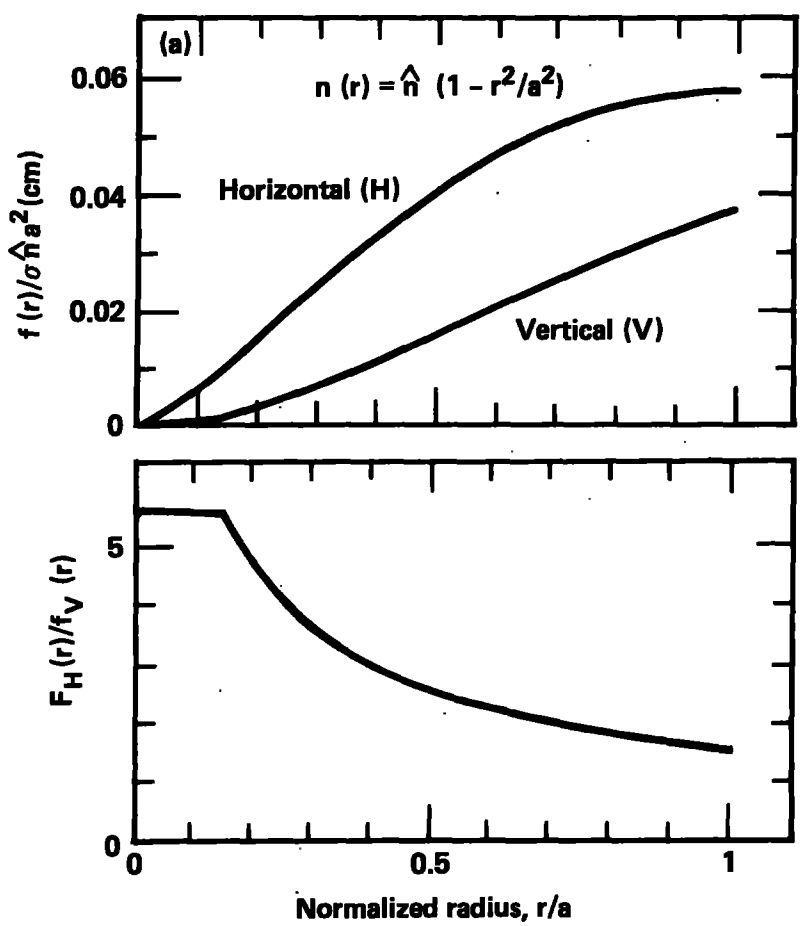

Fig. 11. Guiding-center trapping fraction for a parabolic plasma density profile, $\hat{n}(r) = n\ (1 - r^2/a^2)$.

where ρ is the gyroradius offset of the beam-injected ions and c/2 is the half-width of the beam profile. The hot-ion density is assumed to be uniform inside this core radius and is neglected outside this radius.

We first treat the build-up of hot ions as though charge exchange were the only important loss. Ion-ion scattering, electron drag, and equilibration with warm ions will be treated subsequently. In the presence of beam injection and charge exchange loss, the equation for hot-density build-up is

$$V_h \frac{dn_h}{dt} = \frac{(n_w + n_h)\,\sigma_i + n_w\,\sigma_{cx}}{(n_w + n_h)(\sigma_i + \sigma_{cx})} \left[1 - \exp - (\sigma_i + \sigma_{cx})\,\ell(n_w + n_h)\right] \frac{I_b}{e}$$

$$- n_0 \langle\sigma v\rangle_{cx}\, n_h\, V_h \quad , \tag{17}$$

where n_w and n_h are the respective warm- and hot-ion densities (assumed to be uniform in the core plasma), r = 9 cm, $\sigma_i = 3.5 \times 10^{-16}$ cm^2, $\sigma_{cx} = 1.3 \times 10^{-15}$ cm^2, $\langle\sigma v\rangle_{cx} = 1.3 \times 10^{-7}$ cm^3, n_0 is the neutral density in the core plasma, V_h is the hot-ion volume, ℓ = 13.4 cm (the beam path length inside the core plasma), and I_0 is the incident-beam current. The exponential factor in Eq. (17) describes attenuation of the beam as it passes through the plasma.

The cold neutral-density n_0 and beam current I_b that reach the core plasma are attenuated by the warm plasma outside 9- cm radius. The background pressure near the region of beam injection in the central cell is expected to be $\sim 2 \times 10^{-6}$ Torr for previously attained wall reflux coefficients (see Table 4). Therefore, the external molecular density is $n^{ext}_{molecular} \simeq 6.7 \times 10^{10}$ cm^{-3}. These molecules are dissociated into 2.5 eV Franck-Condon atoms, giving an atomic neutral density at the plasma edge of

$$n_{atom} = n_{molecule} \times \frac{v_{mol}}{v_{atom}} \times 2\,TR \quad ,$$

where TR is the fraction incident atoms converted to inward-moving Franck-Condon atoms, the factor of 2 accounts for 2 atoms per molecule, $v_{mol} = 1.25 \times 10^5$ cm/s is the speed of 300 degree kelvin molecules and $v_{atom} = 1.55 \times 10^6$ cm/s is the speed of 2.5 eV Franck-Condon atoms. For an edge-plasma electron temperature $T_e \simeq 10$ eV, TR $\simeq 0.4$[3] and

$$n_{atom} = 0.065\, n_{molecule} \quad . \tag{18}$$

These inward moving Franck-Condon atoms are further attenuated before reaching the core plasma. A fairly good approximation to gas-code calculations of this attenuation is

$$\exp - \sigma_{FC} \int_{r=9cm}^{20\ cm} \hat{n}_w \left(1 - \frac{r^2}{a^2}\right) dr \quad ,$$

$$= \exp - 0.25\, \sigma_{FC}\, \hat{n}_w\, a \quad , \tag{19}$$

where $\sigma_{FC} = 7.0 \times 10^{-14}$ cm^2. Similarly, we estimated the attenuation of beam current by warm plasma. In Table 6, we summarize the results for beam current and Franck-Condon density for warm-plasma densities n_w of 10^{12}, 3×10^{12}, and 10^{13} cm^{-3}. An incident beam current of 140 A is assumed.

In the low density limit Eq. (17) reduces to

$$V_h \frac{dn_h}{dt} = [(n_w + n_h)\, \sigma_i \ell - n_w\, \sigma_{cx}\, \ell] \frac{I_b}{e} - n_0 \langle \sigma v \rangle_{cx}\, n_h\, V_h \quad . \tag{20}$$

Exponential build-up of n_h requires that the coefficient of n_h in Eq. (20) be positive or that

$$n_0 < \frac{\sigma_i \ell}{V_h \langle \sigma v \rangle_{cx}} \frac{I_b}{e} \quad . \tag{21}$$

If the neutral density is so small that the exponentiation condition in Eq. (21) is met, the hot-ion density can build up on itself even with no warm plasma present, $n_w = 0$. Otherwise, the build-up will be sensitively tied to the warm plasma that is present. For a hot-ion plasma dominated by charge exchange, the plasma length will be close to the beam-injection length (average value $\ell_{inj} = 200$ cm) and the hot-plasma volume V_h is equal to $\pi\ (9)^2\ (200) = 5.1 \times 10^4$ cm^3. Inserting this value and an I_b value of 140 A in Eq. (21) gives the bound required for exponentiation,

$$n_0 < 6.2 \times 10^8\ \text{cm}^{-3} \quad , \tag{22}$$

which is evidently well below what can be achieved if no warm plasma present.

The hot-ion density, calculated as a function of neutral density by solving Eq. (17) in steady state, is shown in Fig. 1 for warm-plasma densities n_w of 0, 10^{12}, 3×10^{12}, and 10^{13} cm^{-3}. We used a hot-plasma volume V_h of

Table 6. Beam current I_b, warm-plasma density n_w, and Franck-Condon density at the core plasma n_0 (FC).

n_w (cm^{-3})	n_0 (FC) (cm^{-3})	I_b (A)
1×10^{12}	3.05×10^{9}	136
3×10^{12}	1.5×10^{9}	127
1×10^{13}	1.3×10^{8}	102

5.1×10^4 cm^3, which is appropriate for a charge-exchange-loss dominated plasma. Before concluding what hot-ion densities we can achieve, we must consider the limits imposed by ion-ion scattering, electron drag, and equilibration with warm ions.

We first consider a hot-ion central-cell plasma with loss dominated by ion-ion scattering. Classically, the time required for deuterium ions with energy E_h (keV) to scatter by an angle $\delta\theta$ is given by

$$n\tau_{ii} = 1.74 \times 10^{10} \left(\frac{2\delta\theta}{\pi}\right)^2 E_h^{3/2} \quad . \tag{23}$$

To properly treat loss of central-cell ions by pitch-angle scattering, we must take into account the fact that charge-exchange reactions of beam-injected atoms with the hot-ion distribution are continually pulling the pitch-angle distribution back to the injection angle. A similar problem was treated,[4] where the problem of hot-ion loss by electron drag into the ambipolar hole in 2XIIB was considered. Rewriting his result, we find the effective ion-ion scattering time is given by

$$\tau_{ii}^{eff} = \tau_{cx}^{b} \left[e^{\tau_{ii}/\tau_{cx}^{b}} - 1\right] \quad , \tag{24}$$

where τ_{ii} is the ion-ion scattering time in Eq. (23) and τ_{cx}^{b} is the mean time for replacement of a hot-ion by charge-exchange on a beam injected atom, which is given explicity by

$$\frac{n_h V_h}{\tau_{cx}^{b}} = \frac{n_h \sigma_{cx}}{(n_w+n_h)(\sigma_i+\sigma_{cx})} \left[1 - \exp - (\sigma_i+\sigma_{cx})\ell(n_w+n_h)\right] \frac{I_b}{e} \quad . \tag{25}$$

The equation for build-up of hot-ion density with ion-ion scattering becomes

$$V_h \frac{dn_h}{dt} = \frac{(n_w + n_h)\,\sigma_i + n_w\sigma_{cx}}{(n_w + n_h)\,(\sigma_i + \sigma_{cx})} \left[1 - \exp - (\sigma_i + \sigma_{cx})\,\ell\,(n_w + n_h)\right] \frac{I_b}{e}$$

$$- n_h V_h \frac{n_h + n_h}{(n\tau)_{ii}^{eff}} \quad . \tag{26}$$

The average hot-ion energy is determined by hot-ion power balance, which in steady state is given by

$$\frac{n_h V_h}{\tau_{ii}^{eff}} (E_b - E_h) + \frac{n_h \sigma_{cx}}{(n_w + n_h)\,\sigma_i + n_w \sigma_{cx}} \frac{n_h V_h}{\tau_{ii}^{eff}} (E_b - E_h)$$

$$- \frac{n_h V_h E_h}{\tau_{hw}} - \frac{n_h V_h E_h}{\tau_{ie}} = 0 \quad , \tag{27}$$

where the electron drag time $\tau_{ie} = 4.2 \times 10^7 \, [T_e \, (eV)]^{3/2}/(n_w + n_h)$ and the equilibration time τ_{hw} between hot and warm ions is

$$\tau_{hw} = \frac{6.2 \times 10^9 \, E_h(keV)^{3/2}}{n_w} \quad .$$

The power balance equation can be rearranged to give

$$\frac{E_b}{E_h} = 1 + \frac{(n_w + n_h)\,\sigma_i + n_w \sigma_{cx}}{(n_w + n_h)\,(\sigma_i + \sigma_{cx})} \left(\frac{\tau_{ii}^{eff}}{\tau_{ie}} + \frac{\tau_{ii}^{eff}}{\tau_{hw}} \right) \quad . \tag{28}$$

Equations (26) and (28) are solved in steady state to give the hot-ion density n_h and the average energy E_h as functions of the warm-plasma density n_w and the electron temperature T_e. To evaluate the ion-ion scattering rate in Eq. (23), we take the average pitch angle of beam-injected ions at the midplane, $\langle \theta_{inj} \rangle = 66°$, and subtract the loss cone angle to the mirror throats, $\theta_{LC} = \sin^{-1} 1/(7.33)^{1/2} = 22°$, to give a scattering angle $\delta\theta = 44°$ for a lost ion. Furthermore, we take an effective flux-tube length ℓ of 500 cm (corresponding to the full distance between mirrors), which gives a hot-plasma volume $V_h = \pi(9)^2 \, (500) = 1.27 \times 10^5$ cm^3. In these calculations we assume that neutral density in the vicinity of the gas box is reduced by the higher fueling efficiency of the low-energy neutral source[5] so that ions are not lost by charge exchange when they pitch-angle scatter to the z-axis location of the gas box.

In Fig. 1 the solutions to Eqs. (26) and (28) (for electron temperature $T_e = \infty$, 500, 250, and 125 eV and for warm-plasma density $n_w = 0$, 10^{12}, 3×10^{12}, and 10^{13} cm^{-3}) are shown by the dashed lines. For a given electron temperature, ion-ion scattering imposes a limit on hot-ion density that is

relatively insensitive to the warm-plasma density, because the increased trapping is offset by increased scattering and drag.

The results of Fig. 1 allow us to estimate the predicted experimental density n_h and the conditions under which n_h is limited by charge exchange or scattering. Operating points for charge-exchange loss and the neutral densities expected are indicated by heavy black dots on the charge-exchange loss curves for the warm-plasma densities of 1 and 3 x 10^{12} cm^{-3}. For n_w = 1 x 10^{13} cm^{-3}, neutral attenuation is so large and the expected neutral density so low (1.3 x 10^{8} cm^{-3}) that the corresponding operating point is off the graph is the upper left-hand corner. Therefore, for n_w = 1 x 10^{12} cm^{-3}, n_h is predicted to be 1.1 x 10^{12} cm^{-3} and limited by charge-exchange loss. If n_w is increased to 3 x 10^{12} cm^{-3}, the predicted n_h increases sharply to somewhere above 4 x 10^{12} cm^{-3}, where the effects of electron temperature and ion-ion scattering become dominant, and the acvhieved hot-density n_h is relatively insensitive to n_w. If the electron temperature T_e = 500 eV, which is near the proposal value of 600 eV, the hot-ion density is expected to reach values of approximately 7 to 9 x 10^{12} cm^{-3}. On the other hand, if T_e = 125 eV, a hot-ion density of 3.5 to 5.5 x 10^{12} cm^{-3} is expected.

The hot-ion parameters expected for various combinations of (n_w, n_0, and T_e) are summarized in Table 1. Besides parameters already discussed, we also include the hot-ion beta β_h for B_c = 3.0 kG; the power P_{hw} from the hot to warm ions,

$$P_{hw} = \frac{n_h V_h E_h}{\tau_{hw}^E}$$

$$= 2.6 \times 10^{-26} \frac{n_w n_h V_h}{E_h(\text{keV})^{1/2}} \text{ Watts} \quad ; \tag{29}$$

the power P_{he} from the hot ions to electrons,

$$P_{he} = \frac{n_h V_h E_h}{\tau_{ie}^E}$$

$$= 3.8 \times 10^{-24} (n_w + n_h) \frac{n_h V_h E_h(\text{keV})}{T_e(\text{eV})^{3/2}} \text{ Watts} \quad ; \tag{30}$$

and the hot-ion power P_{h0}^{cx} lost to charge exchange on background neutral density,

$$P_{h0}^{cx} = \frac{n_h V_h E_h}{\tau_{cx}^{gas}}$$

$$= 1.6 \times 10^{-16} \frac{n_h V_h E_h(keV)}{\tau_{cx}^{gas}} \text{ Watts} \quad . \tag{31}$$

APPENDIX. NOMENCLATURE AND SYMBOLS USED

Symbols	Definition
B_c	magnetic field, central cell
C	conductance
e	electron charge
f	wall reflux parameter
f_H	horizontal beam-absorption-fraction, horizontal orientation
f_v	vertical beam-absorption-fraction, vertical orientation
I_b	neutral beam current
ℓ	beam-absorption path length
ℓ_{inj}	axial beam-injection length
n_w	warm-plasma density
n_h	hot-ion density
n_0	cold neutral density in the core plasma
$n^{ext}_{molecular}$	external molecular density
p_{ion}	probability that an atom incident as a molecule on plasma surface is ionized
P	steady-state pressure for plasma
P_{hw}	power from hot to warm ions
P_{he}	power from hot ions to electrons
P^{cx}_0	hot-ion power lost to charge exchange on background neutral density

Symbols	Definition
Q_s	streaming gas input
Q_D	diffuse-beam gas input
Q_B	beam-dump reflux
Q_w	wall reflux
r	radius
S	pumping speed
S_p	black surface pumping speed of the plasma
T_e	electron temperature
TR	fraction incident atoms converted to inward moving Franck-Condon atoms
v	molecular velocity
v_{mol}	speed of 300-K molecules
v_{atom}	speed of 2.5-eV Franck-Condon atoms
V_h	hot-ion volume, hot-plasma volume
β_h	hot ion beta
γ_w	wall-reflux coefficient, number of D_2 molecules released from the wall per incident atomic D°
σ_i	ionization cross section
σ_{cx}	charge exchange cross section
ρ	ion gyroradius

Symbols	Definition
τ_{ii}^{eff}	effective ion-ion scattering time
τ_{ie}	electron drag time
τ_{hw}	equilibration time between hot and warm ions
τ_{cx}^{b}	mean time for replacement of a hot ion by charge exchange on a beam-injected atom
θ_{LC}	loss cone angle to the mirror throats
$\delta\theta$	scattering angle
Subscripts	
cx	charge exchange
FC	Franck-Condon
h	hot
H	horizontal
V	vertical
p	plasma
w	wall

REFERENCES

1. W. C. Turner, W. E. Nexsen, and R. G. Kerr, Modifications of Beam Gas Inputs to TMX-U Plasma Region During March/April 1983, Lawrence Livermore National Laboratory, Livermore, CA, memorandum (May 18, 1983).

2. W. C. Turner, W. E. Nexsen, S. L. Allen et al., Gas Pressure in the End Plug Regions of the TMX-U Thermal Barrier Experiment, Lawrence Livermore National Laboratory, Livermore, CA, UCRL-89938 Rev. 1 (June 19, 1984), to be published in Dec. 1984 issue of J. of Vacuum Science and Technology.

3. W. E. Nexsen and W. C. Turner, Lawrence Livermore National Laboratory, Livermore, CA, memorandum (May 3, 1984).

4. M. E. Rensink, Lawrence Livermore National Laboratory, Livermore, CA, memorandum (1978).

5. W. C. Turner, A Low Energy Neutral Source for Fueling the Central Cell Core Plasma of TMX-U, Lawrence Livermore National Laboratory, Livermore, CA, UCID-20259 (April 23, 1984).

4625v/MM